PARAMETRIC STUDY AND OPTIMIZATION OF CAST Al-Si ALLOY HEAT EXCHANGER USING TAGUCHI METHOD

by

Jian JIAO, Qinxin ZHAO*, Yungang WANG, Shifeng DENG, and Huaishuang SHAO

Key Laboratory of Thermo-Fluid Science and Engineering,
Ministry of Education, Xi'an Jiao Tong University, Xi'an, Shaanxi, China

Original scientific paper
https://doi.org/10.2298/TSCI230507181J

A 3-D numerical model of staggered pin fin array in cast Al-Si alloy heat exchanger was established. For further structural optimization, seven geometric parameters were studied by Taguchi method, including diameter, width, transverse spacing, longitudinal spacing, offset distance, slit length, and row number. The 32 cases with different geometric parameters were simulated numerically. The heat transfer characteristics, flow resistance characteristics, and overall performance were fully discussed. The diameter and transverse spacing have important influence on heat transfer characteristics, and the structural parameters that affect the resistance characteristics are diameter, longitudinal spacing and slit length. Then analysis of variance shows that diameter and transverse spacing have greater effects on the overall performance than other five parameters. At last, the optimized structure of staggered pin fin array was obtained, and $j/f^{1/3}$ increased by 1% to 3% for volume flow rate in the range from 0.03 to 0.11 m^3/s.

Key words: flue gas, Taguchi method, numerical simulations, heat exchanger, heat transfer characteristics

Introduction

With the world energy revolution and global attention to air quality, as well as adjustment of China's energy mix, the development of new energy efficient utilization technology is becoming increasingly important [1]. It is significant for energy saving and emission reduction to gradually replace coal-fired boilers with gas-fired boilers. Therefore, the cast Al-Si alloy heat exchanger has gradually been receiving attention. On the one hand, it adopts ultra-low nitrogen premixed combustion to replace the traditional atmospheric combustion, which can realize the full mixing of air and fuel and reduces the combustion temperature to control the emission of nitrogen oxides. On the other hand, the casting process and the Al-Si alloy with excellent low-temperature corrosion resistance also change the structure and material of the traditional equipment.

At present, the research on cast Al-Si alloy heat exchanger is insufficient and focuses on its material structure behavior. Wankhede *et al*. [2] experimentally studied the effects of

*Corresponding author, e-mail: zhaoqx@mail.xjtu.edu.cn

pouring temperature and cold wall thickness on Al-Si castings and established a regression model of tensile strength and hardness based on predictors. Tyagunov *et al*. [3] experimentally studied the effect of melting conditions on the microstructure of Al30 alloy, and a physical model of solidification of Al-Si alloy was proposed. In the operation level of the cast Al-Si alloy heat exchanger, Cao *et al*. [4] found that concentration of NO_x is the highest when the thermal load rate of Al-Si gas boiler is 90%. Liu *et al*. [5] experimentally believed that the post-premix system is more suitable for small condensing boilers, and optimal excess air coefficient is 1.23. Banifateme *et al*. [6] proposed a loss method for estimating thermal efficiency and exergy efficiency of condensing gas boilers based on ASME PTC 4.1 and proved that condensing gas boilers can improve boiler energy efficiency, but exergy efficiency is not significantly improved.

The convection heating surface of cast Al-Si alloy heat exchanger consists of staggered pin fin. Simoneau and Vanfossen [7] studied the cooling influence of staggered and linear pin fin arrays. The total heat transfer coefficient of short fin is lower than that of long fin, as found by comparing the *H/D* ratio. Subsequently, Metzger *et al*. [8] studied the effects of longitudinal and transverse distances on heat transfer and pressure drop of pin fin structures and conducted experiments on staggered and linear pin fin structures, respectively. The results showed that the average area heat transfer coefficient depends on the flow direction and transverse distance. Wirtz and Colban [9] found that staggered pin-fined surface has higher heat transfer coefficient and resistance coefficient than the in-line pin-fined surface. Sahoo and Roul [10] numerically studied different extended heat exchange surfaces, especially for conductive and nonconductive rectangular and square fins, whose average Nusselt number is about 36% higher than that of pin-fin plate.

Considering that there are many structural variables for cast Al-Si alloy heat exchanger, Taguchi method is adopted, which is an effective optimization design method. It uses an orthogonal table to arrange experimental schemes and uses analysis of variance to evaluate and simulate product quality. At present, some scholars have also gradually applied Taguchi method in the study of heat transfer enhancement. Alinejad and Esfahani [11] and Alinejad and Fallah [12] simulated the maximum heat transfer rate in isothermal rotating cylinders by using Taguchi method and obtained the optimal process parameters based on *S/N* analysis. Kotcioglu *et al*. [13] conducted experiments with an orthogonal array of L25, using the Taguchi method to determine the optimal design parameters of the rectangular air tube heat exchanger, and achieved the minimum pressure drop and the maximum heat transfer. Feng *et al*. [14] optimized the flow and heat transfer of H-fin tubes, and obtained the optimal configuration by Taguchi method, respectively. Other researchers have also used the method to optimize studies on different subjects [15-19]. The advantage of Taguchi method is that when multiple factors affect a certain result, the influence degree of each factor can be obtained, so that researchers can grasp the main contradiction and carry out design optimization purposefully.

Numerical simulation of staggered pin fin structure of cast Al-Si alloy heat exchanger is carried out. In this structure, there are seven relatively independent variables. Therefore, Taguchi method is adopted for parameter optimization, and each variable has four levels. Then, the effect of the aforementioned key dimensions on the heat transfer and resistance characteristics was calculated and analyzed. The parameters were diameter, width, transverse spacing, longitudinal spacing, offset distance, slit length, and row number. At the same time, the overall performance of different staggered pin fin structures was investigated, and the contribution of various variables to the overall performance is analyzed. Then, the optimal structure was obtained under the consideration of strengthening heat transfer and reducing resistance.

Geometrical configuration and numerical methods

Modeling and computational domains

The geometric structure of cast Al-Si alloy heat exchanger is shown in fig. 1. Figure 1(a) is the real product image of cast Al-Si alloy heat exchanger. Figures 1(b) and 1(c) are side view and front view of convection heating surface of heat exchanger, respectively. The convection heating surface is composed of staggered cylindrical pin fin with periodic height changes. Cooling water enters the heat exchanger from the bottom, and the flue gas flows past the pin fin arrays vertically.

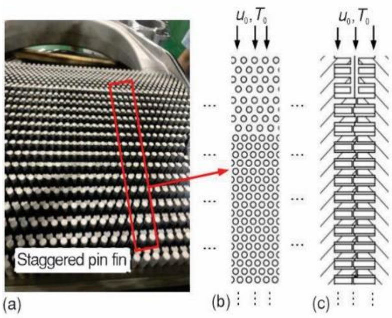

Figure 1. Staggered pin-fined structure; (a) real product image, (b) side view, and (c) front view

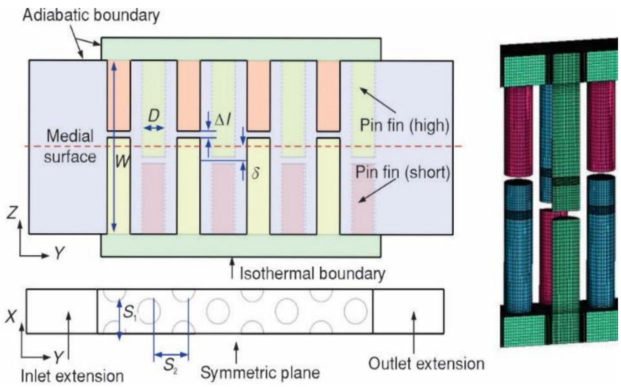

Figure 2. Boundary conditions and meshes

In the 3-D orthogonal coordinate system, *X*-direction is the direction perpendicular to the incoming flow, *Y*-direction is the flow direction of the flue gas, and *Z*-direction represents the height direction of pin fin, as shown in fig. 2. Considering that pin-fined structure has array characteristics along the *X*-direction, the part between the two pin fins can be used as the calculation region. To ensure flow uniform at the inlet and no backflow at the outlet, it is necessary to add inlet and outlet extension sections, respectively. The upper and lower walls are the isothermal boundary outside the substrate, and the left and right sides are symmetric boundaries. After being fully developed in the inlet extension section, the flue gas exchanges are heated with the pin fin and flow out of the outlet extension section after several staggered pin fin rows.

Governing equations and data reduction

To consider the heat exchanger under the proposed range of Reynolds number, the gas flow is assumed to be 3-D, incompressible, steady, and turbulent. The situation of low-Reynolds number should be considered. From the basic analysis of heat transfer, the thermal resistance on the water side and on the baseplate are much smaller than that on the flue gas side. Thus, the baseplate can be considered to a constant temperature state. However, due to the large fin area, the temperature variation of its surface is not negligible. Therefore, the computation of the solid region at the fin is conjugate, requiring simultaneous calculation of the solid and surrounding fluid.

The governing equation has the following tensor form:

$$\nabla\left(\rho\vec{\mathrm{V}}\varphi\right)=\nabla\left(\Gamma_{\varphi}\mathrm{grad}\varphi\right)+S_{\varphi} \tag{1}$$

where the variable φ can represent the velocity components for momentum equation and represent 1 for conservation equation. The Γ_φ and S_φ stand for diffusion coefficient and source term corresponding to φ. The k-ω based SST model adopts:

$$\frac{\partial}{\partial t}(\rho k)+\frac{\partial}{\partial x_j}(\rho k u_j)=\frac{\partial}{\partial x_j}\left[\left(\mu+\frac{\mu_t}{\sigma_k}\right)\frac{\partial k}{\partial x_j}\right]+P_k-\beta'\rho k\omega+P_{kb} \tag{2}$$

$$\frac{\partial}{\partial t}(\rho\omega)+\frac{\partial}{\partial x_j}(\rho\omega u_j)=\frac{\partial}{\partial x_j}\left[\left(\mu+\frac{\mu_t}{\sigma_k}\right)\frac{\partial \omega}{\partial x_j}\right]+\frac{\alpha\omega}{k}P_k-\beta\rho\omega^2+P_{\omega b} \tag{3}$$

where ρ is the density, u – the velocity vector, and P_k – the production rate of turbulence.

The energy equation is shown as:

$$\frac{\partial}{\partial t}(\rho E)+\frac{\partial}{\partial x_i}\left[u_i(\rho E+p)\right]+\frac{\partial}{\partial x_i}\left(\lambda_{\text{eff}}\frac{\partial T}{\partial x_i}\right) \tag{4}$$

where E is the total energy and $\lambda_{\text{eff}} = \lambda + \lambda_t$, where λ_t is the turbulent thermal conductivity.

The flue gas composition in the calculation is measured according to the actual composition of natural gas after combustion. The composition is shown in tab. 1.

Table 1. Flue gas composition for numerical simulation

Composition	CO_2	H_2O	N_2	O_2	Total
Volume fraction [%]	7.38	16.09	71.06	5.47	100

Enthalpy flow at the inlet, H_{in}, and outlet, H_{out}, positions in computational domain is obtained by FLUENT calculation. Then, the heat transfer rate for the flue gas side can be calculated according to:

$$Q = H_{\text{in}} - H_{\text{out}} \tag{5}$$

Then, the heat transfer coefficient, h, can be calculated from eq.(6), where A_{tot} is the total surface area, and ΔT is the logarithmic mean temperature difference:

$$h=\frac{Q}{A_{\text{tot}}\Delta T} \tag{6}$$

$$\Delta T=\frac{T_{\text{out}}-T_{\text{in}}}{\ln\left(\dfrac{T_{\text{out}}-T_{\text{w}}}{T_{\text{in}}-T_{\text{w}}}\right)} \tag{7}$$

where T_{in} and T_{out} represent the temperature of inlet and outlet and T_{w} – the temperature of the baseplate.

The heat transfer coefficients are expressed in the dimensionless form by the Nusselt numbers, and Re = $u_{\max}D_{\text{h}}/\nu$, where D_{h} is the hydraulic diameter in the minimum flow cross-section of the computational domain:

$$\text{Nu}=\frac{hD_{\text{h}}}{\lambda} \tag{8}$$

$$D_{\text{h}}=4\frac{A_{\min}}{C_{\text{h}}}=\frac{\dfrac{2\left[S_1W-D(W-\Delta l)\right]}{W}}{n+S_1+W-\Delta l} \tag{9}$$

In addition, Colburn factor, j, and the friction factor, f, are:

$$j = \mathrm{St}(\mathrm{Pr})^{2/3} = \frac{\mathrm{Nu}}{\mathrm{Re}\,\mathrm{Pr}^{1/3}} \tag{10}$$

$$f = \frac{\tau_\mathrm{w}}{\dfrac{\rho u_\mathrm{max}^2}{2}} = \frac{\dfrac{\Delta p D_e}{4L}}{\dfrac{\rho u_\mathrm{max}^2}{2}} = \frac{\Delta p D_e}{2\rho u_\mathrm{max}^2 L} \tag{11}$$

where Δp is the pressure drop of the computational domain and ρ – the density at the qualitative temperature.

Grid independence and computational validation

The structural parameters of staggered pin-fin model used for grid independence verification are shown in tab. 2

Table 2. Geometric parameters of the staggered pin fin for model validation

D [mm]	W [mm]	S_1 [mm]	S_2 [mm]	δ [mm]	Δl [mm]	N
7	50	14	14	2	2	8

To verify the grid independence, the models with the grid number of 202000, 395000, 774000, 1222000, 1590000, and 2570000 cells are calculated, respectively. The obtained factor j and f are shown in fig. 3, which indicates that the calculation results almost do not change when the number of grids exceeds 1590000. Thus, the grid system with 1590000 cells is adopted, so that the calculation time and accuracy can be considered.

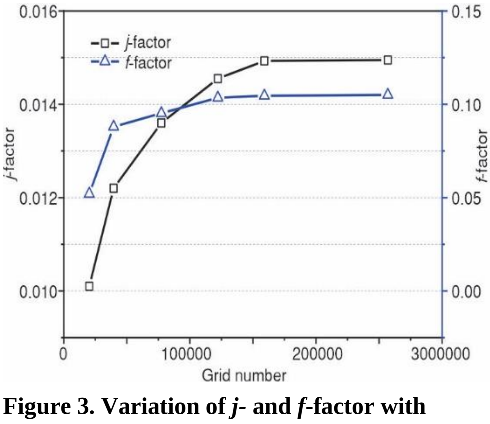

Figure 3. Variation of *j*- and *f*-factor with grid number (Re = 2236)

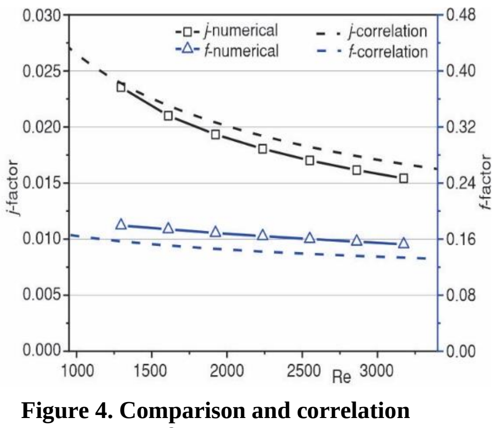

Figure 4. Comparison and correlation between *j* and *f* numerical simulation

To verify the numerical reliability, j and f are compared with the experimental correlations provided by Kays and London [20]. The results are displayed in fig. 4 and the corresponding Reynolds number is 1255 to 3074. Besides, the average deviation for j factor is 5.6%, and the average deviation for f factor is 14.9% compared with the experimental correlation. Thus, the numerical calculation results are in good agreement with the experimental results.

Simulation design for optimization with Taguchi method

Optimized target selection

The first step of Taguchi method optimization is to select appropriate optimized targets. Heat transfer and flow resistance are the generally two key characteristics for heat exchangers, so j-factor and f-factor are used to characterize them respectively [21-24]. However, the flow resistance of the structure tends to increase as the heat transfer enhancing. Thus, to evaluate overall performance of heat exchangers, a new dimensionless number JF is adopted [25]:

$$JF = \frac{\dfrac{j}{j_0}}{\left(\dfrac{f}{f_0}\right)^{1/3}} \tag{12}$$

where j_0 and f_0 represent the j and f factor of the reference heat exchanger. When JF is 1, the increase in friction loss generated by heat exchange benefit is worthwhile.

Control factors and Taguchi orthogonal array design

The control factors are seven structural parameters of the staggered pin-fin plate for cast Al-Si alloy heat exchanger, which are diameter, width, transverse spacing, longitudinal spacing, slit length, offset distance, and the total number of pin-fin rows, respectively. Four levels are designed and shown in tab. 3. Besides, inlet boundary conditions for all cases are set up as a constant volume flow (q_m = 0.06 m^3/s, T_{in} = 473 K).

Table 3. Different levels of seven structural factors

Code	Factors	Unit	Level-1	Level-2	Level-3	Level-4
A	Diameter, D	mm	6	7	8	9
B	Width, W	mm	46	50	54	58
C	Transverse spacing, S_1	mm	5	6	7	8
D	Longitudinal spacing, S_2	mm	5	6	7	8
E	Offset distance, δ	mm	0	1	2	3
F	Slit length, Δl	mm	1	2	3	4
G	Row number, N	–	8	10	12	14

Orthogonal array is an important part of Taguchi method. By arranging different levels under different factors according to orthogonality, a representative working condition of evenly dispersed, neatly comparable can be obtained, thereby effectively reducing the number of experiments. Considering that the research has seven factors, and each factor has four levels, there will be 4^7 (=16384) combinations in total if a comprehensive simulation is conducted. However, only 32 times are required by orthogonal combination. At the same time, considering that the number of repeated factors at each level is the same in the orthogonal experiment, it is reasonable to analyze and compare the influence degree of these seven factors.

Therefore, based on seven factors and four levels, the orthonormal table $L_{32}(4^7)$ is selected, and the distribution of each factor and level is shown in tab. 4. The number 1, 2, 3, and 4 represent levels 1, 2, 3, and 4, respectively.

Table 4. The orthogonal table of $L_{32}(4^7)$ for staggered pin-fin

	Case number															
Factors	1	2	3	4	5	6	7	8	9	10	11	12	13	14	15	16
A	1	1	1	1	1	1	1	1	2	2	2	2	2	2	2	2
B	1	1	2	2	3	3	4	4	1	1	2	2	3	3	4	4
C	1	2	3	4	1	2	3	4	3	4	1	2	3	4	1	2
D	1	2	4	3	3	4	2	1	4	3	1	2	2	1	3	4
E	1	4	1	4	2	3	2	3	3	2	3	2	4	1	4	1
F	1	4	2	3	4	1	3	2	4	1	3	2	1	4	2	3
G	1	3	3	1	2	4	4	2	2	4	4	2	1	3	3	1
	Case number															
Factors	17	18	19	20	21	22	23	24	25	26	27	28	29	30	31	32
A	3	3	3	3	3	3	3	3	4	4	4	4	4	4	4	4
B	1	1	2	2	3	3	4	4	1	1	2	2	3	3	4	4
C	3	4	1	2	3	4	1	2	1	2	3	4	1	2	3	4
D	1	2	4	3	3	4	2	1	4	3	1	2	2	1	3	4
E	4	1	4	1	3	2	3	2	2	3	2	3	1	4	1	4
F	2	3	1	4	3	2	4	1	3	2	4	1	2	3	1	4
G	4	2	2	4	3	1	1	3	3	1	1	3	4	2	2	4

Mean analysis of signal-to-noise ratio

After obtaining raw data under 32, tab. 4, structures through numerical simulations, the optimized targets (j, f, and JF) are converted into log-based signal-to-noise ratio (SNR) form. For cast Al-Si alloy heat exchanger, the j factor represents the heat transfer characteristics, the f factor represents the flow resistance characteristics, and the JF factor comprehensively evaluates the overall characteristic. Therefore, the larger the result for j and JF, the better, while the smaller the result for f, the better. The corresponding SNR formulas are:

$$\mathrm{SNR_L} = -10\lg\left(\frac{1}{n}\sum_{i=1}^{n}\frac{1}{y_i^2}\right) \tag{13}$$

$$\mathrm{SNR_S} = -10\lg\left(\frac{1}{n}\sum_{i=1}^{n}y_i^2\right) \tag{14}$$

where y is the optimized target calculated according to the numerical simulation and n – the number of repeated experiments. In addition, the total mean value of SNR is expressed by k, and the formula is as:

$$k = \frac{1}{m}\sum_{i=1}^{m}\eta_i \tag{15}$$

where m is the total number of cases, m = 32 and η_i – the SNR of case i. The average SNR at each level is the arithmetic mean of the SNR at the corresponding level of each factor.

In addition, R is the range of the average $\mathrm{SNR_S}$ at all levels of each factor. To evaluate the influence degree of all 7 structural parameters, contribution ratio C_r is introduced as:

$$R = k_{\max,i} - k_{\min,i} \tag{16}$$

$$C_\mathrm{r} = \frac{k_{\max,i} - k_{\min,i}}{\sum_{i=1}^{4}\left(k_{\max,i} - k_{\min,i}\right)} \tag{17}$$

Result and discussion

Parameter analysis of j and f

Intuitive analysis is usually used to obtain the influence of different factors on the target and contribution rate. All 32 cases in the orthogonal array are numerically simulated, and the *j* factor, *f* factor, and their respective SNR_S are obtained. The results after further processing of the original data are displayed in tab. 5, and the influences of various structural parameters are as shown in tab. 6 and fig. 5.

Table 5. Target results and SNR_S for cases

Case No.	1	2	3	4	5	6	7	8	9	10	11
$j \times 10^2$	1.641	1.672	2.138	2.434	1.500	1.969	2.152	2.851	1.533	2.027	1.121
SNR-*j*	–35.7	–35.5	–33.4	–32.3	–36.5	–34.1	–33.3	–30.9	–36.3	–33.9	–39.0
$f \times 10^2$	5.661	3.342	3.067	3.057	3.338	4.40	3.603	4.250	3.072	4.690	4.242
SNR-*f*	24.94	29.52	30.27	30.29	29.53	27.14	28.87	27.43	30.25	26.58	27.45
Case No.	12	13	14	15	16	17	18	19	20	21	22
$j \times 10^2$	1.496	1.983	1.983	1.251	1.481	1.386	1.527	0.997	1.090	1.402	1.751
SNR-*j*	–36.5	–34.1	–34.1	–38.1	–36.6	–37.2	–36.3	–40.0	–39.3	–37.1	–35.1
$f \times 10^2$	4.042	5.720	4.072	4.004	3.445	4.555	3.973	5.395	3.658	3.740	3.766
SNR-*f*	27.87	24.85	27.80	27.95	29.26	26.83	28.02	25.36	28.73	28.54	28.48
Case No.	23	24	25	26	27	28	29	30	31	32	
$j \times 10^2$	1.004	1.375	0.721	0.972	1.186	1.456	0.830	1.029	1.324	1.328	
SNR-*j*	–40.0	–37.2	–42.8	–40.2	–38.5	–36.7	–41.6	–39.8	–37.6	–37.5	
$f \times 102$	4.536	6.735	3.632	4.186	4.931	5.979	4.683	4.827	6.112	3.663	
SNR-*f*	26.87	23.43	28.80	27.56	26.14	24.47	26.59	26.33	24.28	28.72	

Table 6. Factorial effects for SNR-*j* and SNR-*f*

Target	Level	A	B	C	D	E	F	G
j	1	–33.97	–37.24	–39.21	–36.54	–36.81	–36.16	–36.56
	2	–36.05	–36.96	–37.40	–36.76	–36.74	–36.63	–36.73
	3	–37.77	–36.53	–35.92	–36.85	–36.79	–37.15	–36.86
	4	–39.35	–36.40	–34.60	–36.99	–36.80	–37.20	–36.99
	R	5.38	0.85	4.61	0.45	0.07	1.04	0.43
	Cr [%]	41.95	6.59	35.91	3.50	0.57	8.13	3.34
	Rank	1	4	2	5	7	3	6
f	1	28.50	27.81	27.19	26.29	27.49	26.63	27.30
	2	27.75	27.57	27.48	27.13	27.46	27.87	27.38
	3	27.03	27.41	27.50	27.93	27.46	28.44	27.60
	4	26.61	27.10	27.72	28.53	27.48	28.45	27.61
	R	1.89	0.71	0.54	2.24	0.02	1.82	0.31
	Cr [%]	25.06	9.46	7.16	29.73	0.32	24.11	4.15
	Rank	2	4	5	1	7	3	6

According to the calculated average SNR of each control factor, the corresponding main effect diagram is drawn to illustrate the influence of the control factor as shown in figs. 6 and 8, respectively.

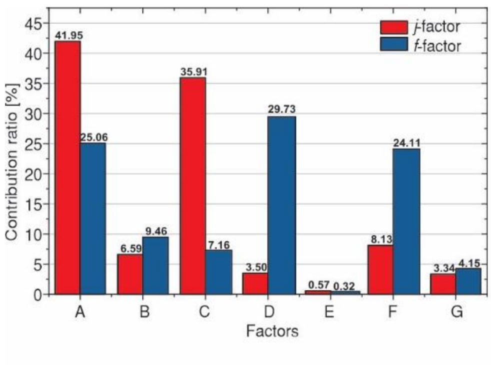

Figure 5. Contribution ratio of *j*-factor and *f*-factor

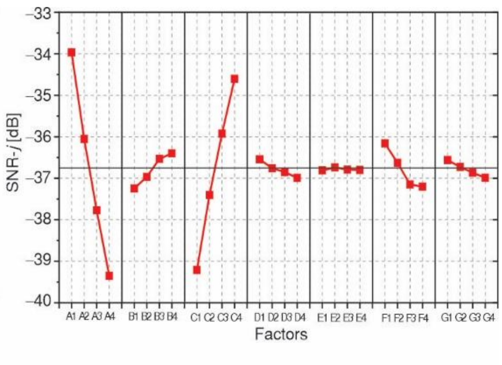

Figure 6. Main effect plots for SNR-*j*

Table 6 and fig. 6 show that the order of the parametric validity of j is A > C > F > B > D > G > E. Diameter (A), transverse spacing (C), and slit length (F) have obvious effects on j factor with contribution ratios of 41.95%, 35.91%, and 8.13%, respectively. The reason are: The decrease of diameter (A) and the increase of transverse spacing (C) lead to the increase of hydraulic diameter, which represents the degree of freedom of fluid-flow. The larger the hydraulic diameter is, the larger the Reynolds number will be. Thus, the flow is more turbulent, and the j factor increases. Moreover, the position of the slit is just in the mainstream of flue gas. So, the heat transfer in the central area of the mainstream flue gas is weakened with increasing slit length (F), resulting in the decrease of j. The total contribution ratios of these three parameters are above 85%, indicating that the influences of other parameters are less important. Therefore, diameter (A), transverse spacing (C), and slit length (F) should be considered when optimizing heat transfer characteristics. It is also shown that offset distance (E) nearly has no effect on the heat transfer characteristics under selected conditions. Thus, the combination with the maximum value of SNR-*j* can be considered as the optimal combination (A1B4C4D1E2F1G1) from fig. 6 for heat transfer characteristics.

However, if the amount of change between the various levels of one factor is affected by another factor, then there is an interaction between the two factors, and the conviction of the results will be weakened. Therefore, the interaction contour among the top three dominant factors is shown in fig. 7. The more regular the change of contour line, the less interaction between the two structural factors, and the stronger the independence. As can be seen from fig. 7, contour lines of diameter (A) and transverse spacing (C) change most regularly, indicating that these two factors are completely independent of each other in the effects on factor j. However, the contour changes between diameter (A) and slit length (F) are chaotic, indicating that there is a certain interaction between these two factors. Besides, the contour lines of transverse spacing (C) and slit length (F) show a certain change in upper and lower layers, indicating that these two factors are generally relatively

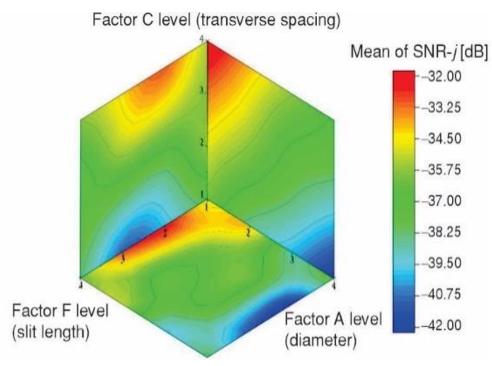

Figure 7. Diagram of the interaction of three main structural factors for *j* factor

independent, but there is a small amount of interaction. Moreover, the change of slit length (F) has little influence on the factor *j*, which is also consistent with the results above (R_F = 3, c_F = 8.13%).

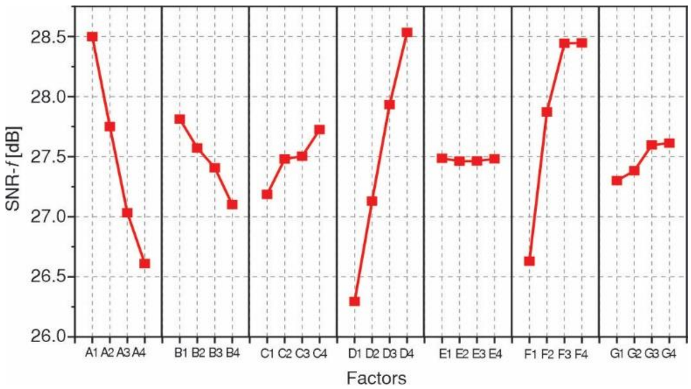

Figure 8. Main effect plots for SNR-*f*

As can be seen from tab. 6 and fig. 8, the order of parameter validity of *f* is D > A > F > B > C > G > E. Longitudinal spacing (D) has the strongest effect on SNR-*f* contributing 29.73%. This is because the longitudinal spacing directly affects the total length of the fluid in the flow direction. Thus, when longitudinal spacing increases, the *f* factor decreases, and the SNR-*f* increases. In addition, diameter (A) and slit length (F) also have significant effect on SNR-*f* with contribution ratios of 25.06% and 24.11%. These phenomena can be explained as: On the one hand, as the diameter (A) increases, the contact area between the fin and the fluid increases significantly, resulting in a sharp increase in surface friction. On the other hand, the increase of the slit length leads to part of flue gas flowing to the outlet without bypassing the pin fin, so that the f factor decreases, and the resistance characteristic improves. The total contribution ratios of these three factors amount to 78.90%, indicating that the three factors have the most significant influence on the flow resistance characteristic of pin-fin plate. Figure 8 also reveals that offset distance (E) has almost no effect on flow resistance characteristics.

The three dominant factors for *f* factor are diameter (A), longitudinal spacing (D), and slit length (F). Therefore, interactive contours are shown as fig. 9. It can be seen from the variation of contour lines that longitudinal spacing (D) has a strong interaction with diameter (A), while slit length (F) has no significant interaction with the others.

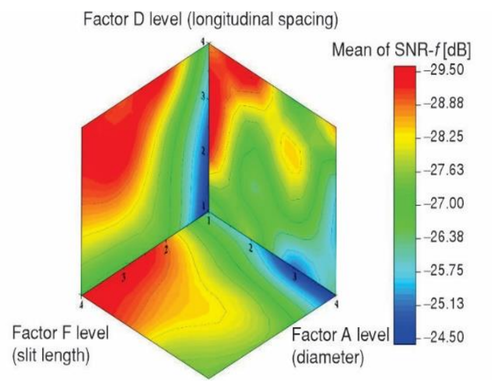

Figure 9. Diagram of the interaction of three main structural factors for *f* factor

In conclusion, the combination with the maximum value of SNR-*f* can be considered as the optimal combination of flow resistance characteristics. It can be seen that the best SNR-*f* combination is A1B1C4D4E1F4G4 from fig. 8, while the best SNR-*j* combination is A1B4C4D1E2F1G1. Therefore, heat transfer and flow resistance characteristic cannot be optimized at the same time.

Parameter analysis optimization of JF

Intuitive analysis

The JF can be used to evaluate the overall performance. Factorial effects for SNR-*JF* are shown in tab. 7 and fig. 10. It shows that the rank order is A > C > B > F > G> D > E.

Table 7. Factorial effects for SNR-*JF*

Target	Level	A	B	C	D	E	F	G
JF	1	2.91	–0.590	–2.766	–0.393	–0.267	–0.400	–0.076
	2	0.582	–0.391	–0.859	–0.333	–0.201	0.047	–0.218
	3	–1.37	–0.015	0.626	–0.155	–0.253	–0.286	–0.281
	4	–3.09	0.0176	2.021	–0.096	–0.256	–0.338	–0.401
	R	6.01	0.61	4.79	0.30	0.07	0.45	0.32
	Cr [%]	47.93	4.85	38.17	2.37	0.52	3.57	2.59
	rank	1	3	2	6	7	4	5

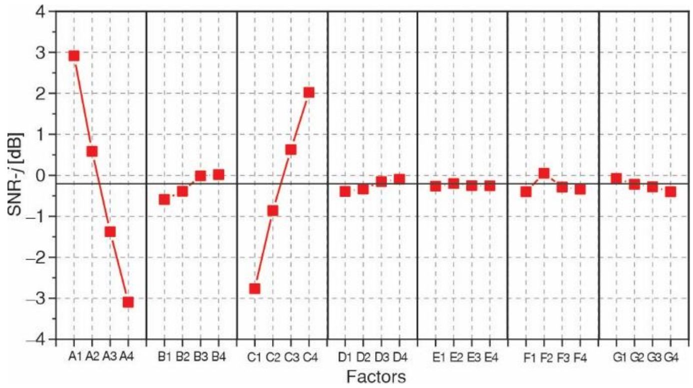

Figure 10. Main effect plot for SNR-*JF*

As can be seen from fig. 10, diameter (A) has the greatest influence on SNR-*JF*, whereas longitudinal spacing (D), offset distance (E), and row number have minor effects. The contribution ratios of diameter (A) and transverse spacing (C) amounts up to 86.1%, indicating that these two parameters are of great significance for the design and optimization of thermal performance. Comparing SNR-*JF* values under different levels, the optimal combination of A1B4C4D4E2F2G1 is easily obtained, which has the best overall performance than the others.

By comparing fig. 10 with figs. 6 and 8, the rationality of the influence of various factors on SNR-*JF* can be proved. As the diameter increases from A1 to A4, SNR-*j* and SNR-f decrease, causing SNR-*JF* to drop rapidly. Considering that the variations of *j* and *f* factor is similar to the change of transverse spacing (C), the change of SNR-*JF* is similar. Besides, SNR-*JF* increases slightly as slit length (F) increases from F1 to F2. However, it drops when slit length increases from F2 to F4. Although heat transfer characteristics get worse to some extent, flow resistance characteristics are also improved when slit length increases from F1 to F2 as shown in fig. 8. However, when slit length further increases to F4, the heat transfer characteristic deteriorates further, whereas the flow resistance increases slowly. Thus, the benefits from flow resistance are counteracted.

The ANOVA and effect of factors

The ANOVA for *JF* is carried out and the results are shown in tab. 8. The *f* ratios in tab. 7 and their PCR are considered to identify the significance level of the variables. A larger variance indicates a more effective factor. Table 8 shows that the most effective on the *JF* value is the diameter with 59.99% of contribution ratio. The second significant variable is transverse spacing (35.31%). The other variables have minor effects on *JF*.

Table 8. Analysis of variance

Variation of source	DoF	Sum of squares (SS)	Mean of squares (MS)	F ratio	P value	Contribution
A	3	2.3183	0.7728	109.42	0	59.994
B	3	0.0366	0.0122	1.72	0.225	0.946
C	3	1.3646	0.4549	64.41	0	35.314
D	3	0.0079	0.0026	0.37	0.776	0.203
E	3	0.0010	0.0003	0.05	0.985	0.027
F	3	0.0574	0.0191	2.71	0.101	1.486
G	3	0.0078	0.0026	0.37	0.777	0.202
Error(e)	10	0.0706	0.0071			1.828
Total	31	3.8642				100.00

In order to verify the statistical reliability of the above calculated results, it is necessary to perform an F-test at 95% confidence level, and the calculated F-value are compared to the F-test table. A factor is considered significant if its calculated F-value is greater than that of the standard F-test table. The results show diameter (A) and transverse spacing (C) are statistically significant. Therefore, these two parameters need to be prioritized during design and optimization. Analysis of variance further verifies the correctness of intuitive analysis.

In intuitive analysis, Taguchi method is used to obtain the optimal level combination of *JF*. However, this result is based on the assumption that the effects of different parameters are additive. The premise of this hypothesis is that the interaction between parameters is insignificant, but in fact there may be interaction between parameters. Therefore, an additive confirmation test is used to evaluate the interaction effect. The specific practice is to compare the optimal SNR-*JF* value predicted according to the main effect with the calculated value. When the difference between the two is within ±2 dB, the interaction can be considered not significant. ANOVA showed that diameter (A), transverse spacing (C), and slit length (F) of *JF* are statistically significant. Therefore, the predicted SNR-*JF* is calculated by:

$$SNR = \overline{SNR} + \left(SNR_{\mathrm{A}} - \overline{SNR}\right) + \left(SNR_{\mathrm{C}} - \overline{SNR}\right) + \left(SNR_{\mathrm{F}} - \overline{SNR}\right) \tag{18}$$

where $\overline{SNR}$ is the total average of SNR-*JF*, whereas SNR_{A}, SNR_{C}, SNR_{F} are the optimal level average SNR-*JF* of factors A, C, F.

The comparison of the predicted optimal value with the calculated value is shown in fig. 11. The predicted optimal values and calculated values show the same trend. Therefore, the overall performance of cast Al-Si alloy heat exchanger can be predicted by using these three factors (diameter, transverse spacing, and slit length).

Verification for the optimal combination

The optimal combination is A1B4C4D4E2F2G1 based on the above conditions, but it is under the condition of constant volume flow (q_{m} = 0.06 m^3/s). Therefore, the optimized combination must be validated over a wide range of volume flow. To ensure that the chosen case is representative, case 8 (A1B4C4D1E3F2G2) and case 4 (A1B2C4D3E4F3G1), which have the highest $j/f^{1/3}$ output, are selected, and compared. Figure 12 shows the variation of $j/f^{1/3}$ with volume flow for staggered pin fin with different parametric combinations. At a certain range of volume flow, the $j/f^{1/3}$ of the optimal combination is higher than those of the other cases. When volume flow is between 0.03 m^3/s and 0.11 m^3/s, the $j/f^{1/3}$ of the optimal combination increases by 1% to 3% compared with case 8, whose $j/f^{1/3}$ is the greatest in 32 numerical cases. Thus, the optimal combination has obvious superiority, thereby proving the reliability of the method.

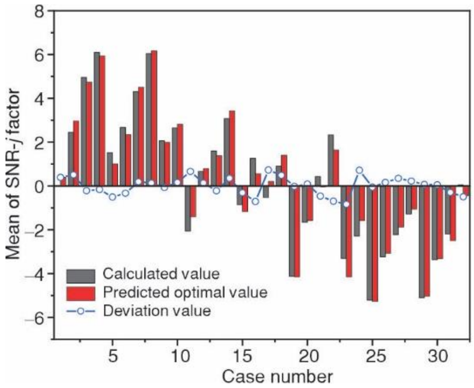

Figure 11. comparison of the predicted optimal value with the calculated value

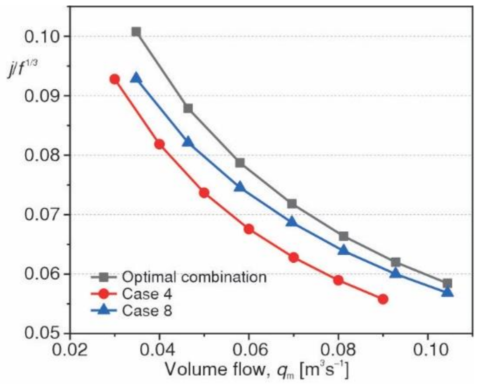

Figure 12. Variations of $j/f^{1/3}$ for staggered pin fin with different parametric combinations

Conclusions

The influences of geometric parameters on heat transfer characteristics, flow resistance characteristics, and overall performance of cast Al-Si alloy heat exchanger are studied. The validity of different parameters for the three objectives is evaluated, and geometry is optimized using Taguchi method to obtain the best overall performance. The main conclusions are as follows.

- Seven structural parameters are considered for optimization, including diameter, width, transverse spacing, longitudinal spacing, offset distance, slit length, and row number. Diameter, transverse spacing, and slit length have the greatest influence on heat transfer characteristics, with contribution rates of 41.95%, 35.91%, and 8.13%, respectively. The other four parameters have little influence on heat transfer characteristics. In terms of flow resistance characteristics, diameter, longitudinal spacing, and slit length have great effects on flow resistance characteristics, and their contribution rates are 25.06%, 29.73%, and 24.11%, respectively, whereas the effects of the other four parameters are negligible.
- The influence of each parameter on the overall performance is studied. The diameter and transverse spacing are the dominant parameters. The sum of contribution rates is 86.1%. Therefore, the design and optimization of cast Al-Si alloy heat exchanger should prioritize these two parameters in the case of limited time and investment.
- Taking *JF* value as the objective of comprehensive evaluation, Taguchi method is used to optimize the geometric structure of staggered pin fins. The optimal combination is A1B4C4D4E2F2G1. The confirmed additivity shows that the interaction is negligible, so Taguchi method is reasonable for optimization. Finally, $j/f^{1/3}$ increased by 1% to 3% for

volume flow rate in the range from 0.03 m^3/s to 0.11 m^3/s, compared to the best of the 32 groups.

Acknowledgment

This research was supported by the National Natural Science Foundation of China (NO.51876165 and NO.52276085).

References

[1] He, Y., *et al*., Experimental Study on Heat Transfer Enhancement Characteristics of Tube with Cross Hollow Twisted Tape Inserts, *Applied Thermal Engineering, 131* (2018), Feb., pp. 743-749
[2] Wankhede, D. M., *et al*., Experimental Investigations of Mechanical Properties and Microstructural Characterization of Aluminum-Silicon Alloy Castings, *Proceedings*, International Conference on Intelligent Manufacturing and Automation, Springer, Singapore, 2019
[3] Tyagunov, G., *et al*., Influence of Melt Preparing Technology on the Structure of Cast Aluminum-Silicon Alloy, *IOP Conference Series: Materials Science and Engineering, 572* (2019), 012048
[4] Cao, W., *et al*., Performance of Casting Aluminum-Silicon Alloy Condensing Heating Exchanger for Gas-Fired Boiler, *Heat and Mass Transfer, 54* (2018), 7, pp. 1951-1960
[5] Liu, F., *et al*., Performance and Emissions of Pre-Mixed and Post-Mixed Combustion Systems with a Casting Aluminum-Silicon Alloy (CASA) Condensing Gas Boiler, *Heat and Mass Transfer, 56* (2020), 2, pp. 651-662
[6] Banifateme, M., *et al*., Development of a Loss Method for Energy and Exergy Audit of Condensing Hot Water Boilers, *Journal of Energy Resources Technology, 143* (2021), 5, 052104
[7] Simoneau, R. J., Vanfossen, G. J., Effect of Location in an Array on Heat-Transfer to a Short Cylinder in Cross-Flow, *Journal of Heat Transfer, 106* (1984), 1, pp. 42-48
[8] Metzger, D. E., *et al*., Effect of Pin Shape and Array Orientation on Heat Transfer and Pressure Loss and Pin Fin Arrays, *Gas Turbines Power, 106* (1984), 1, pp. 252-257
[9] Wirtz, R. A., Colban, D. M., Comparison of the Cooling Performance of Staggered and In-Line Arrays of Electronic Packages, *Journal of Electronic Packaging, 118* (1996), 1, pp. 27-30
[10] Sahoo, L. K., Roul, M. K., CFD Analysis on Heat Transfer Through Different Extended Surfaces, *Heat Transfer, 49* (2020), 8, pp. 4820-4833
[11] Alinejad, J., Esfahani, J. A., Taguchi Design of Three Dimensional Simulations for Optimization of Turbulent Mixed Convection in a Cavity, *Meccanica, 52* (2017), 4-5, pp. 925-938
[12] Alinejad, J., Fallah, K., Taguchi Optimization Approach for Three-Dimensional Nanofluid Natural Convection in a Transformable Enclosure, *Journal of Thermophysics and Heat Transfer, 31* (2017), 1, pp. 211-217
[13] Kotcioglu, I., *et al*., Experimental Investigation for Optimization of Design Parameters in a Rectangular Duct with Plate-Fins Heat Exchanger by Taguchi Method, *Applied Thermal Engineering, 50* (2013), 1, pp. 604-613
[14] Feng, Y., *et al*., Optimization of H-type Finned Tube Heat Exchangers with Combinations of Longitudinal Vortex Generator, Dimples/Protrusions and Grooves by Taguchi Method, *International Communications in Heat and Mass Transfer, 143* (2023), 106709
[15] Jamshidi, N., *et al*., Experimental Analysis of Heat Transfer Enhancement in Shell and Helical Tube Heat Exchangers, *Applied Thermal Engineering, 51* (2013), 1-2, pp. 644-652
[16] Mamourian, M., *et al*., Optimization of Mixed Convection Heat Transfer with Entropy Generation in a Wavy Surface Square Lid-Driven Cavity by Means of Taguchi Approach, *International Journal of Heat and Mass Transfer, 102* (2016), Nov., pp. 544-554
[17] Manigandan, S., *et al*., Effect of Hydrogen and Multiwall Carbon Nanotubes Blends on Combustion Performance and Emission of Diesel Engine Using Taguchi Approach, *Fuel, 276* (2020), 118120
[18] Huang, S., *et al*., Multifactor Optimization of Medium and Deep U-Type Borehole Heat Exchanger Design Using Taguchi Method, *Geothermics, 109* (2023), 102644
[19] Dagdevir, T., Multi-Objective Optimization of Geometrical Parameters of Dimples on a Dimpled Heat Exchanger Tube by Taguchi Based Grey Relation Analysis and Response Surface Method, *International Journal of Thermal Sciences, 173* (2022), 107365
[20] Kays, W., London. A. L., Compact Heat Exchangers (2nd ed.), McGraw-Hill Book Company, Inc., New York, USA, 1966

[21] Wang, H., *et al*., Parametric Study and Optimization of H-Type Finned Tube Heat Exchangers Using Taguchi Method, *Applied Thermal Engineering, 103* (2016), June, pp. 128-138
[22] Tang, X. Y., Zhu, D. S., Flow Structure and Heat Transfer in a Narrow Rectangular Channel with Different Discrete Rib Arrays, *Chemical Engineering and Processing-Process Intensification, 69* (2013), July, pp. 1-14
[23] Kim, Y., Kim, Y., Heat Transfer Characteristics of Flat Plate Finned-Tube Heat Exchangers with Large Fin Pitch, *International Journal of Refrigeration, 28* (2005), 6, pp. 851-858
[24] Wang, C., Chi, K., Heat Transfer and Friction Characteristics of Plain Fin-and-Tube Heat Exchangers, Part I: New Experimental Data, *International Journal of Heat and Mass Transfer, 43* (2000), 15, pp. 2681-2691
[25] Yun, J. Y., Lee, K. S., Influence of Design Parameters on the Heat Transfer and Flow Friction Characteristics of the Heat Exchanger with Slit Fins, *International Journal of Heat and Mass Transfer, 43* (2000), 14, pp. 2529-2539

Paper submitted: May 7, 2023
Paper revised: July 10, 2023
Paper accepted: July 17, 2023